



Virus passage through compromised low-pressure membranes: A particle tracking model

Frederick W. Pontius^{a,*}, John P. Crimaldi^b, Gary L. Amy^c

^a California Baptist University, 8432 Magnolia Ave, Riverside, CA 92504, United States

^b Department of Civil, Environmental, and Architectural Engineering, University of Colorado, Boulder, CO, United States

^c UNESCO-IHE, Institute for Water Education, Delft, The Netherlands

ARTICLE INFO

Article history:

Received 12 November 2008

Received in revised form 24 May 2011

Accepted 28 May 2011

Available online 25 June 2011

Keywords:

Virus rejection

Particle tracking

Membrane integrity

Microfiltration

Ultrafiltration

ABSTRACT

A Lagrangian particle-tracking model was developed to assess virion passage through compromised membranes. The velocity field created by a hole in the membrane surface is represented by an ideal point sink, superimposed on the uniform flow field through the membrane to describe the flow field resulting from a hole in a flat membrane surface. Catastrophic failure of compromised microfiltration (MF) and ultrafiltration (UF) membranes was observed in laboratory challenge experiments using MS2 and PRD1 phage in 25 mm stirred-cell tests, and predicted by the hydrodynamic model.

A “capture cone” defines the extent of hole influence at the membrane surface. A proportion of viruses within the cone passes through the hole. Membrane resistance has the largest effect on the size and extent of influence of this capture cone. For a given membrane increasing transmembrane pressure (TMP) (and flux) decreases the size of the capture cone and lowers the fraction of particle hole passage.

Brownian motion is an important factor in diffusive transport of viruses. High resistance, low flux conditions generally increase virus passage through a hole and increase the spread of the capture cone. Virus size has a very small effect on hole passage, an increase in virus size slightly lowers passage.

© 2011 Elsevier B.V. All rights reserved.

1. Introduction

Water treatment membrane processes rely on direct and indirect integrity assessment methods which consider the membrane module as a “black box.” That is, if an unacceptable pressure decay or high treated water turbidity is measured, evidence is provided that a membrane integrity problem exists in a module, but the cause of that problem is not revealed [1]. In current practice, a membrane integrity problem is indicated by a single broken fiber within a module or series of modules [2]. Techniques currently do not exist for evaluating the impact on virus rejection of a compromised membrane surface of less than a cut fiber or fiber break (e.g., a very small hole or macro-pore).

Available approaches to membrane integrity assessment do not consider hydrodynamics near the membrane surface [1–3]. Viruses may readily pass through a membrane compromised with a small hole or manufactured with a skewed pore distribution larger than the manufacturer's nominal pore size rating, even though the membrane exhibits acceptable pressure decay. Improved understanding of the effect of small holes and macro-pores is needed to properly

assess the effectiveness of integrity monitoring methods and the potential health significance of virus passage.

Particle-tracking is a useful tool to describe particle or contaminant movement in environmental systems [4–6] offering computational efficiency and simplicity compared to alternative numerical methods [7]. The particle-tracking method does not exhibit any numerical dispersion in the classical sense [4,8] and the computational effort is proportional to the number of particles [9]. Tracking of virion movement in this way allows assessment of individual virus passage through a membrane with a small hole or macro-pore.

A Lagrangian particle-tracking model was developed to track virion passage to and through both uncompromised and compromised low pressure membranes. Particle-tracking in a Lagrangian flow field describes the movement of individual particles (or parcels of water) in a fixed coordinate system as they move through space and time [8,10]. In contrast, modeling within a Eulerian flow field considers fluid motion at specific locations in the space through which the fluid flows through time. Research on virus rejection using low pressure membranes has universally been conducted within an Eulerian flow field by measuring the virus concentration at two points in space (feed and permeate concentrations) and calculating the removal (log rejection) over time. In contrast, a Lagrangian flow field enables tracking of an individual virion as it passes through space (to and through a compromised membrane) over time.

* Corresponding author. Tel.: +1 951 343 4846; fax: +1 951 343 4782.

E-mail addresses: fpontius@calbaptist.edu, fredp@pontiuswater.com (F.W. Pontius).

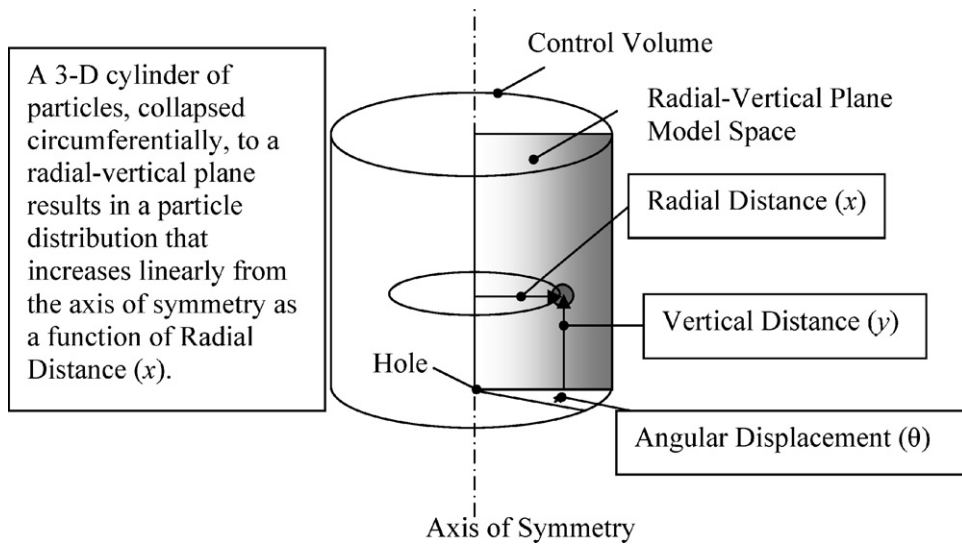


Fig. 1. Particles within a cylindrical control volume.

2. Theory and model framework

Consider a 3-dimensional water volume in the shape of a cylinder on-end, with a membrane surface along the bottom (Fig. 1). A cylindrical hole in the membrane pulls water (and viruses) in toward the center, symmetrically about the centerline. Because of symmetry in the θ -direction, particles within the entire cylinder, or any pie shaped portion of it, may be collapsed down to a model space in the radial-vertical plane (Fig. 1). The resulting radial-vertical plane particle distribution increases linearly as a function of the radial distance (x). An example of such a linear particle distribution of 25,000 particles is provided in Fig. 2.

Within the radial-vertical plane model space, the movement of viruses above a compromised membrane surface may be tracked using Cartesian coordinates (Fig. 3) with the origin at the center, where a small cylindrical hole is located. Viruses are passively transported as water moves downward, in steady, incompressible, two-dimensional flow. Water (and virions) are pulled toward the hole at a radial velocity (v_r). Considering symmetry, the radial velocity of water (and virions) in the radial-vertical plane can be decomposed into an x -direction velocity and a y -direction velocity.

Hence, the velocity of water (and virions) at any point will have two velocity components, u and v . The location (coordinates) of a single virus particle in the water above the membrane is tracked using the following conceptual model:

$$\begin{aligned} \text{Virus position}(x, y) = & \text{Initial virus position}(x_i, y_i) + \text{Change in position caused by flux} \\ & + \text{Change in position caused by hole flow} \\ & + \text{Change in position caused by Brownian motion} \end{aligned} \quad (1)$$

A change in virus position caused by downward flux will occur in the $-y$ direction as a result of the pressure-driven flow of water through the membrane. In addition, water flow through the hole will tend to pull the virus particle toward the hole. Lastly, the particle will move randomly in any direction due to Brownian motion. Equations describing each velocity component are developed in the sections below.

In general, viruses in solution will be passively transported (i.e., carried along) by the water flow. Other than the Brownian motion component, movement of the viruses and of the water will be identical with respect to downward movement caused by the flux and movement caused by flow through the hole.

The water flow to the membrane is symmetrical within the control volume (Fig. 1), following streamlines that converge toward and then pass parallel through the hole. The water does not spin (e.g., does not cross streamlines) as it passes through the membrane and/or hole, a condition referred to as "irrotational" flow. As such, the vorticity (ζ) is zero, or

$$\zeta = \nabla \times \mathbf{V} = 0 \quad (2)$$

where \mathbf{V} is the velocity vector.

As a consequence of irrotationality, a velocity potential, ϕ , may be defined for a general three-dimensional flow. For irrotational flow, the velocity is expressed as the gradient of a scalar function ϕ . In vector form,

$$\mathbf{V} = \nabla \phi \quad (3)$$

For an incompressible fluid,

$$\nabla \cdot \mathbf{V} = 0 \quad (4)$$

Therefore, for flow that is both incompressible and irrotational (Eqs. (3) and (4)),

$$\nabla^2 \phi = 0 \quad (5)$$

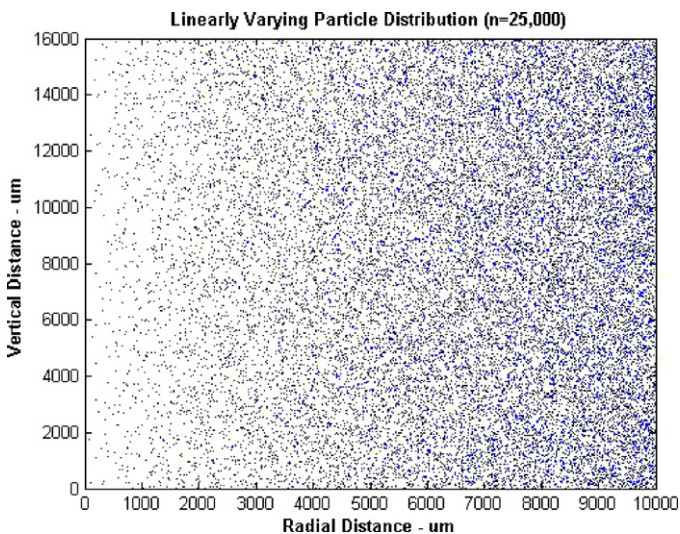


Fig. 2. Example linearly varying particle density distribution.

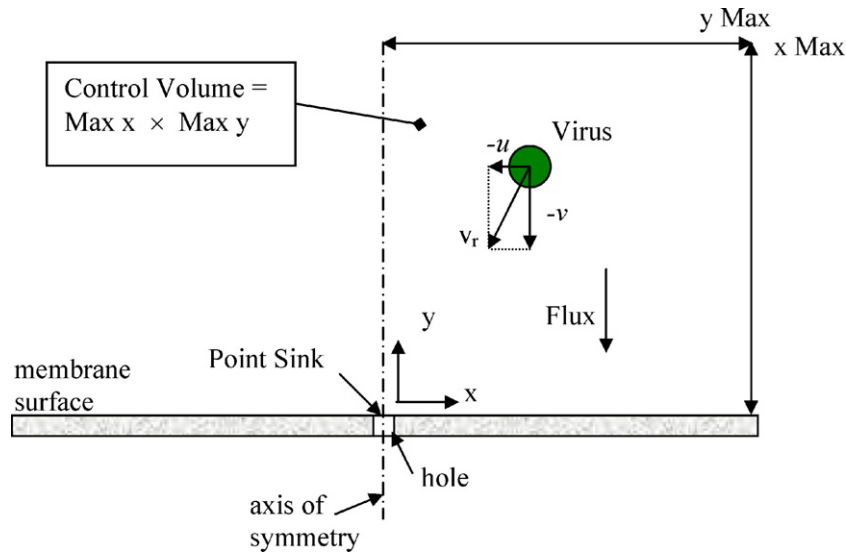


Fig. 3. Particle-tracking model framework.

where $\nabla^2(\cdot) = \nabla \cdot \nabla(\cdot)$ is the Laplacian operator. Flow such as this is governed by Laplace's equation and is commonly called a "potential flow."

For irrotational flow using Cartesian coordinates, the components of the fluid velocity vector may be expressed in terms of a velocity potential scalar function ϕ :

$$u = \frac{\partial \phi}{\partial x}, \quad v = \frac{\partial \phi}{\partial y}, \quad w = \frac{\partial \phi}{\partial z} \quad (6)$$

Using the above gradient operator in cylindrical coordinates (r, θ, z) , the following expressions are derived for the velocity components:

$$v_r = \frac{\partial \phi}{\partial r}, \quad v_\theta = \frac{1}{r} \frac{\partial \phi}{\partial \theta}, \quad v_z = \frac{\partial \phi}{\partial z} \quad (7)$$

2.1. Flux (uniform flow) velocity components

Water above a clean low pressure membrane surface operated in deadend filtration mode at steady state moves toward the membrane surface in a uniform manner. This is the simplest plane flow, called uniform flow. Uniform flow occurs as long as membrane properties are homogeneous across the length of the membrane.

Pressure-driven flow through a flat sheet membrane may be described by considering a uniform flow in the negative y direction as illustrated in Fig. 3. In this case,

$$u = 0 \quad (\text{no velocity in the } x\text{-direction}) \quad (8)$$

$$v = \frac{-Q_y}{A} \quad (9)$$

where Q_y is the flow in y -direction and A is the area of the membrane.

The velocity potential is

$$\frac{\partial \phi}{\partial x} = 0, \quad \frac{\partial \phi}{\partial y} = \frac{-Q_y}{A} \quad (10)$$

Integrating these equations yields

$$\phi = \frac{-Q_y}{A} x + C \quad (11)$$

where C is an arbitrary constant, which is set equal to zero. Therefore, the velocity potential for uniform flow in the y direction is

$$\phi = \frac{-Q_y}{A} x \quad (12)$$

If the hydraulic properties of the membrane are known, or determined in the laboratory, the flow (flux) through the membrane may be calculated using Darcy's Law:

$$J_{tm} = \frac{TMP}{\mu \times R_t} \quad (13)$$

where J_{tm} is the permeate flux at time t ($L/m^2/h$), TMP is the trans-membrane pressure (bar), μ is the water viscosity (cp), and R_t is the total resistance of the membrane ($(\text{bar h } m^2)/(L \text{ cp})$).

The virion is passively transported in the water flow. Hence, the virion (and water) vertical velocity can be determined by calculating the flux (J).

2.2. Hole (point sink) velocity components

A hole in a flat sheet membrane may be represented mathematically as an ideal point sink. Consider a fluid flowing radially inward to an infinitely small point at the origin within a 3-D control volume, as shown in Fig. 4.

Let m be the strength of the ideal point sink expressed as volume rate of flow per time toward the origin (Fig. 5). Then, a 3-D point sink with strength m has the following velocity potential:

$$\phi = \frac{m}{4\pi r} \quad (14)$$

Then,

$$v_r = \frac{\partial \phi}{\partial r} = -\frac{m}{4\pi r^2}, \quad v_\theta = 0, \quad v_z = 0 \quad (15)$$

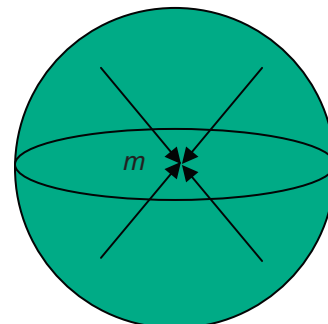


Fig. 4. Ideal point sink.

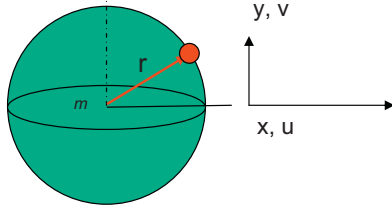


Fig. 5. Point sink model space.

The total inward flux through the sphere of radius r_e may be determined by integrating the radial velocity, v_r (a constant at any r), around the surface, dS :

$$Q_i = \int_S \int v_r dS = v_r \int_S \int dS = -\frac{m(4\pi r_e^2)}{4\pi r_e^2} = -m \text{ (with units volume/time)} \quad (16)$$

Therefore, the flux through the upper half of the sphere is $m/2$.

To determine the velocity components, consider a point (x, y) at radius r and angle θ from an arbitrary x -axis (of an x, y plane with origin at the sphere center) through the center of the sphere:

$$r = (x^2 + y^2)^{1/2} \quad (17)$$

$$\sin \theta = \frac{y}{r} \quad (18)$$

$$\cos \theta = \frac{x}{r} \quad (19)$$

The velocity at point (x, y) is

$$u = v_x = v_r \cos \theta \quad (20)$$

$$v = v_y = v_r \sin \theta \quad (21)$$

Substituting Eqs. (15) and (17)–(19), into Eqs. (20) and (21), and simplifying results in

$$u = -\frac{m}{4\pi} \frac{x}{(x^2 + y^2)^{3/2}} \quad (22)$$

$$v = -\frac{m}{4\pi} \frac{y}{(x^2 + y^2)^{3/2}} \quad (23)$$

where u is the velocity in the x direction (cm/s), v is the velocity in the y direction (cm/s), x is the x coordinate (cm), y is the y coordinate (cm), and m is the point sink strength (cm^3/s).

Potential sinks and sources are useful idealizations of certain real flow fields. At the origin ($x=y=0$) u and v are infinite (Eqs. (21) and (23)), which is not physically possible, representing a mathematical singularity in the flow field. Moving out from the origin, however, the equipotential lines (lines of $\phi = \text{constant}$) for a point sink are concentric circles centered at the origin, as shown by the red arc lines in Fig. 6. The radial velocity (Eq. (15)) is constant along each arc, illustrated in Fig. 6 for an ideal point sink ($m = 10$). The fact that the distance between the circles decreases closer to the origin indicates that the rate of change of the water (and virion) velocity increases as it moves toward the origin (hole). This is also indicated by the radial velocity field vectors (Eq. (15)) shown by the blue arrows in Fig. 6. The vector length (scale up = 4000) is proportional to the local velocity magnitude. Note how quickly these vectors become shorter as the radial distance from the hole increases.

The impact of the hole diminishes significantly only a short distance from the hole. Hence, the hole will have a localized affect on virus transport, depending upon the hole size (e.g., the value of m).

2.3. Brownian motion

Einstein [11] observed that, according to the kinetic (collision) theory of fluids, molecules of water move at random. Therefore, a small particle receives a random number of impacts of random

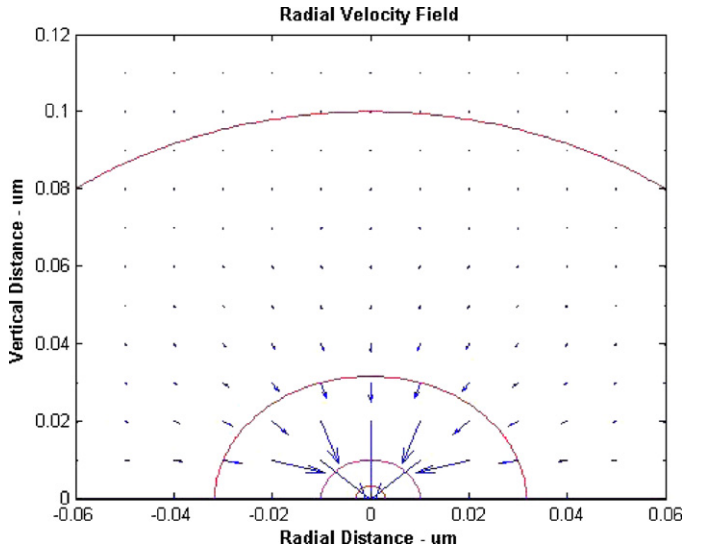


Fig. 6. Radial velocity field for an ideal point sink.

strength and from random directions in any short period of time. The random bombardment by molecules of fluid causes a sufficiently small particle, including viruses, to move.

Consider a virus particle moving randomly in water due to Brownian motion. Since the probability of movement in any direction is equal, the average movement is zero in any direction because the positive and negative displacements are equally probable and effectively cancel one another. This movement is described by calculating the root mean square (rms) displacement. Einstein [11] presented the following relationship for rms displacement caused by Brownian motion, derived by Hiemenz and Rajagopalan [12]:

$$\bar{x}^2 = 2Dt \quad (24)$$

where \bar{x}^2 is the mean square of Brownian motion displacement (cm^2), D is the diffusion coefficient (cm^2/s), and t is the time (s).

The mean Brownian motion displacement in any direction may be estimated by rearranging Eq. (24)

$$x = (2Dt)^{1/2} \quad (25)$$

When the solute size is \gg solvent, Brownian motion of the solute may be equated to the hydrodynamic drag on a particle of equivalent size and shape. For spherical solutes, this results in the Stokes–Einstein equation [11]:

$$D = \frac{kT}{(6\pi\mu r_s)} \quad (26)$$

where D is the diffusivity in dilute solution (m^2/s), k is the Boltzmann's constant (J/K), T is the temperature (K), μ is the solvent viscosity (kg/m/s), and r_s is the solute radius (m).

To determine the mean Brownian motion displacement of a virus particle in any direction, the diffusion coefficient may be calculated using Eq. (26), and then the mean displacement determined for time, t , using Eq. (25).

2.4. Particle position update equation

The position of a virion above a membrane surface is tracked using the particle-tracking method following the general relationship presented above in Eq. (1). The two-dimensional position of a virion x_n is determined from its previous position x_{n-1} using the updating relationship

$$\bar{x}_n = \bar{x}_{n-1} + \bar{u}\Delta t + Z\sqrt{2D\Delta t} \quad (27)$$

where \bar{x}_n is the particle position vector (cm), \bar{u} is the velocity vector at position x_{n-1} (cm), D is the diffusion coefficient, calculated using Eq. (26) (cm^2/s), Z is the a two-dimensional vector of random numbers with mean magnitude zero and variance one, and Δt is the time step (s).

2.5. Particle-tracking model

A particle-tracking model was developed using MatLab (Mathworks, Inc.) to track the location of particles placed within a specified control volume as they move toward a membrane surface with a hole. Taking advantage of symmetry, the control volume (model space) consists of 1/2 of the cross-sectional area of the hole, and extends an equal distance along the radial (x) and vertical (y) direction. Hydrodynamic model simulations were performed tracking the position of virions using Eq. (27) with the following input parameters: hole diameter (μm); particle diameter (nm); transmembrane pressure (TMP); membrane resistance, R_m ($\text{bar m}^2 \text{ h}/(\text{L cp})$); membrane thickness (μm); water temperature ($^\circ\text{C}$); number of particles to be used in the simulation (typically 10,000–25,000); maximum coordinates ($x_{\text{Max}}, y_{\text{Max}}$) and minimum coordinates ($x_{\text{Min}}, y_{\text{Min}}$) representing the control volume; and the time step (s) to be used in the simulation.

For any given membrane resistance (R_m), water temperature, and TMP, the flux through the membrane, expressed as $\mu\text{m}/\text{s}$ or $\text{L}/\text{m}^2 \text{ h}$, is calculated using Darcy's law, Eq. (13). The particle diffusion coefficient (D), expressed as $\mu\text{m}^2/\text{s}$, is calculated for any given particle (virus) size and water temperature, using the Stokes–Einstein equation (26). Experimental studies of MS2 by Möller [13] and MS2 and PRD1 by Badireddy [14] found that the virus diameter calculated using the Stokes–Einstein equation based on measurements of the virus diffusion coefficient corresponded well (within 25%) of the virus diameter determined using scanning electron microscopy (SEM). The difference is due to the fact that diffusion experiments are conducted with hydrated virus spheres (i.e., the hydrodynamic diameter is determined), whereas diameter determinations by SEM do not consider hydration. Möller [13] reported a hydration for MS2 at 2.3 g of water per gram dry virus. Based on these studies, the Stokes–Einstein equation provides a reasonable estimate of the diffusion coefficient for these viruses for modeling purposes.

The hole strength, m , is determined in one of 2 ways. If experimental hydraulic flux data is available, then m is determined using linear regression of the experimental data. Alternatively, the hole strength, m , is determined based on hole flow (Q) calculated using the Hagen–Poiseuille equation:

$$Q = \frac{\pi R^4 \Delta p}{8 \mu l} \quad (28)$$

where Q is the hole flow ($\mu\text{m}^3/\text{s}$), Δp is the pressure drop (Pa), R is the tube radius (μm), l is the tube length (μm), μ is the viscosity (Pa s).

The number of particles simulated are distributed within a radial–vertical plane control volume, randomly in the vertical direction, but linearly distributed in the radial direction. The (x, y) position of each particle is tracked using column vectors, x and y , with a row entry for each particle tracked. The time step (T_{step}) is specified for each simulation based on ensuring that a particle does not miss the hole simply because the computational time step was too big. The minimum time step was determined empirically by running the model with differing time steps to determine the effect on particle passage through the hole. A minimum time step is determined for each control volume simulated.

The position of each particle is tracked using the specified time step. At each time step, the position of each particle is updated using Eq. (27), as it moves from its initial position in the bulk solution to

the membrane surface, or through the hole. The change in position after each time step is determined using the calculated flux, the laboratory-determined hole strength, m , or the calculated m , as discussed above. Brownian motion of each particle is determined using the diffusion coefficient (Eq. (26)) and the mean displacement determined using Eq. (25), multiplied by a random number generated from a normal distribution with a mean of zero and a variance of 1.

The simulation time is based on ensuring that the computations proceed sufficiently long to allow all or almost all of the particles in bulk solution to either reach the membrane surface or reach the hole. The simulation time is calculated based on the maximum y value of the control volume, divided by the calculated flux, then multiplied by a factor of 1.5 to compensate for potential Brownian motion displacement in the $+y$ direction.

If a particle's coordinates reach a distance of 1/2 the particle diameter (D_{part}) or less above the membrane, then that particle is counted as having reached the membrane. If a particle's coordinates reach a distance of 1/2 the particle diameter (D_{part}) or less above the hole, then that particle is counted as having reached the hole. The ultimate fate of each particle (membrane, hole, or bulk solution) is recorded in a separate column matrix allowing a plot to be made showing the particle's initial position and ultimate fate. This plot defines the “capture cone” for the particular conditions of the simulation.

Adaptive time stepping was considered, where by the incremental time would change for each time step, based on achieving a specified degree of error. The computational time necessary for this approach was prohibitive considering that the overall accuracy of the model was not improved compared to the user-specified time step. In addition, a distributed point-sink was also considered and found to be a minor refinement to the approach here. The computational time required was greater with these modifications but the overall results did not significantly differ compared to the overall results presented here.

Virus rejection is calculated for a compromised flat-sheet membrane based on virus passage estimates from the hydrodynamic model as follows:

1. An appropriate control volume is defined around the hole such that the model simulation will define the capture cone within that control volume.
2. Model parameters are defined and entered into the hydrodynamic model, and virus passage is simulated. The “passage” estimate represents the decimal fraction of the particles (virions) within the defined control volume that pass through the hole. This decimal fraction is used to calculate the proportion of virus challenge solution that would pass through the hole during membrane challenge experiments. Virions within the proportion of virus challenge solution that passes through the hole will not be rejected. Since the concentration of virus challenge solution is known from any given experimental data set, the number of virions passing through the hole can be calculated for the defined control volume.
3. The proportion of virus challenge solution within the defined control volume that reaches the membrane surface is rejected based on the virus rejection characteristics of the membrane. Virus rejection characteristics of each membrane are determined from virus challenge studies of uncompromised membranes. Viruses reaching the membrane surface may pass completely through the membrane, or may be rejected. Challenge studies characterize the virus rejection properties for each virus and each membrane in terms of a log-reduction factor. The log-reduction factor is applied to calculate the rejection of viruses reaching the membrane surface.

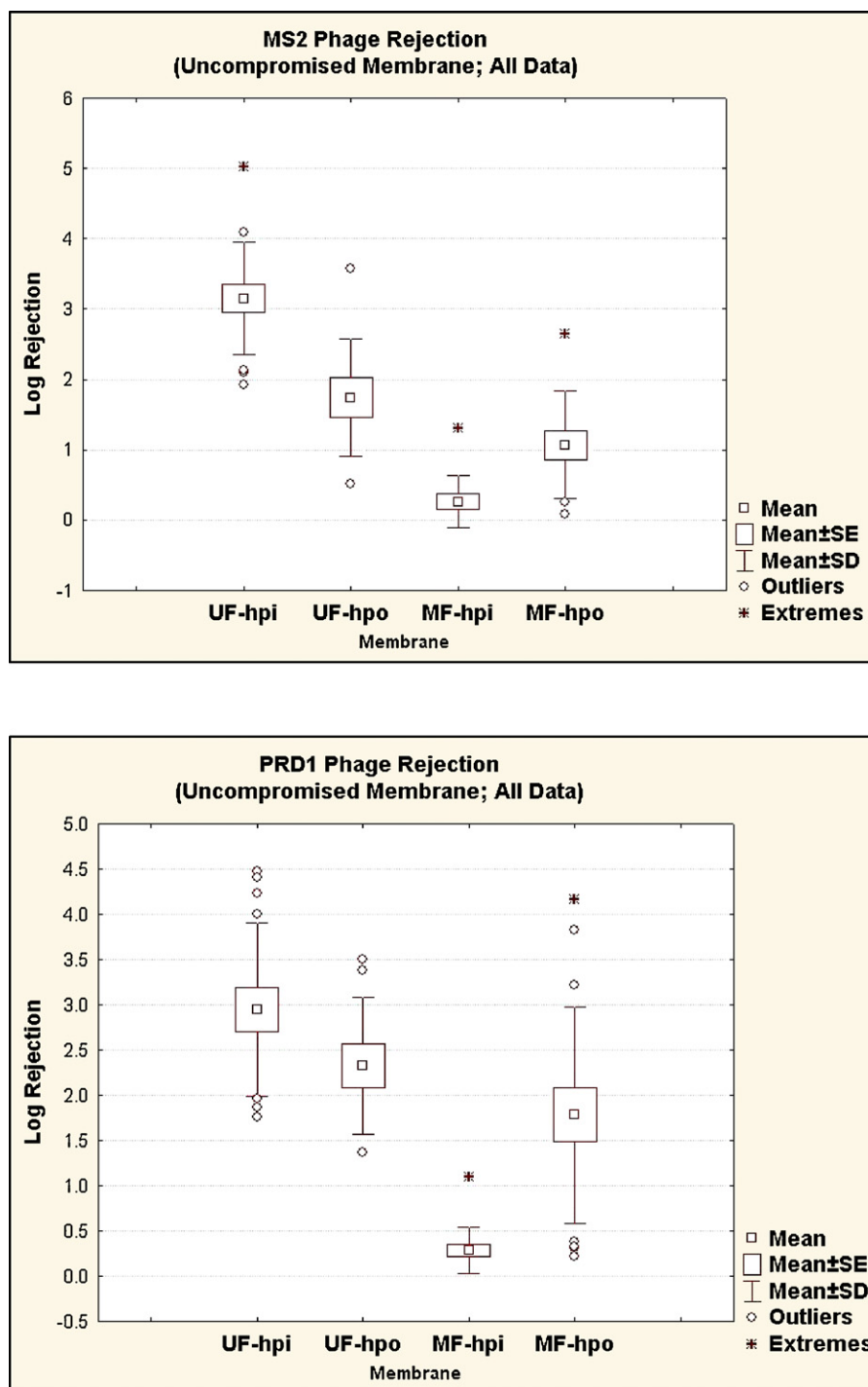


Fig. 7. Phage rejection results.

4. The number of viruses passing through the hole is added to the number of the viruses passing through the membrane to determine the permeate virus concentration. The overall log reduction of viruses for the compromised membrane is calculated.

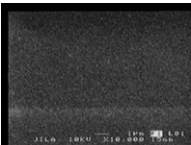
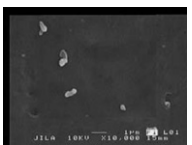
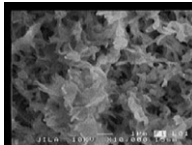
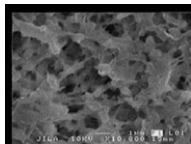
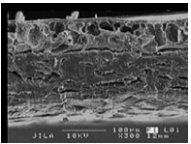
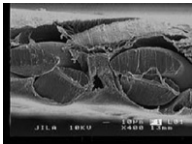
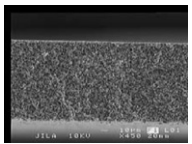
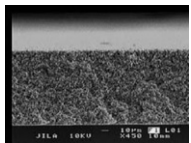
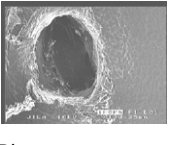
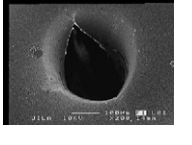
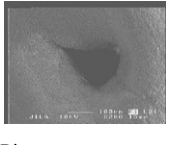
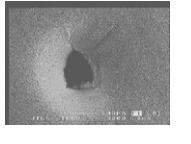
3. Phage rejection experiments

The hydrodynamic model presented above was used to predict to bacteriophage challenge test result for challenge studies using two bacteriophage (MS2 and PRD1), 0.22 μm hydrophilic and hydrophobic polyvinylidene fluoride (PVDF) microfiltration

(MF) membranes, a 100 kD hydrophilic regenerated cellulose (RC) ultrafiltration (UF) membrane, and a 100 kD hydrophobic polyethersulfone (PES) UF membrane. The membranes and bacteriophage were fully characterized according to their surface properties, including hydrophobicity, isoelectric point, surface charge, diameter of the phage, and membrane pore size.

Membrane properties are summarized in Table 1. MS2 and PRD1 challenge studies were performed on uncompromised membranes and membranes compromised with a single needle hole. Membranes were placed in a 25 mm dead-end stirred cell and challenged (without stirring) with a phage solution. The experi-

Table 1
Summary of membrane properties.

Property	Membrane			
	UF-hpi	UF-hpo	MF-hpi	MF-hpo
Type:	Ultrafiltration	Ultrafiltration	Microfiltration	Microfiltration
Model:	Millipore YM100	Orelis PES100	Millipore GVWP	Millipore GVHP
Monomer:	Regenerated Cellulose	Polyethersulphone (PES)	Polyvinylidene fluoride (PVDF)	Polyvinylidene fluoride (PVDF)
Design:	Asymmetric	Asymmetric	Symmetric	Symmetric
Hydrophobicity:	Hydrophilic	Hydrophobic	Hydrophilic	Hydrophobic
Contact angle:	18°	58°	18°	83°
Zeta potential ^a :	−4.8	−33.4	−25.7	−7.4
Mean specific flux @20 °C (L/m ² h bar)	656	374	7157	528
Resistance (R_m) of clean membrane (bar m ² h)/(L cp)	1.52 (10 ^{−3})	2.67 (10 ^{−3})	1.4 (10 ^{−4})	1.89 (10 ^{−3})
Uncompromised membrane nominal pore size:				
	100,000 Da MWCO ^b	100,000 Da MWCO ^b	0.22 μm	0.22 μm
Uncompromised membrane thickness:				
	Total: 180 μm (skin: ~30 μm)	135 μm	125 μm	125 μm
Needle hole:				
	Diameter Mean = 177 μm Std. Dev. = 13 μm	Diameter Mean = 171 μm Std. Dev. = 14 μm	Diameter Mean = 152 μm Std. Dev. = 17 μm	Diameter Mean = 153 μm Std. Dev. = 25 μm

^a At pH = 7.5, $I = 0.01$.

^b 100 kDa molecular weight cut off (MWCO) is equivalent to a nominal pore size of 0.0073 μm [11].

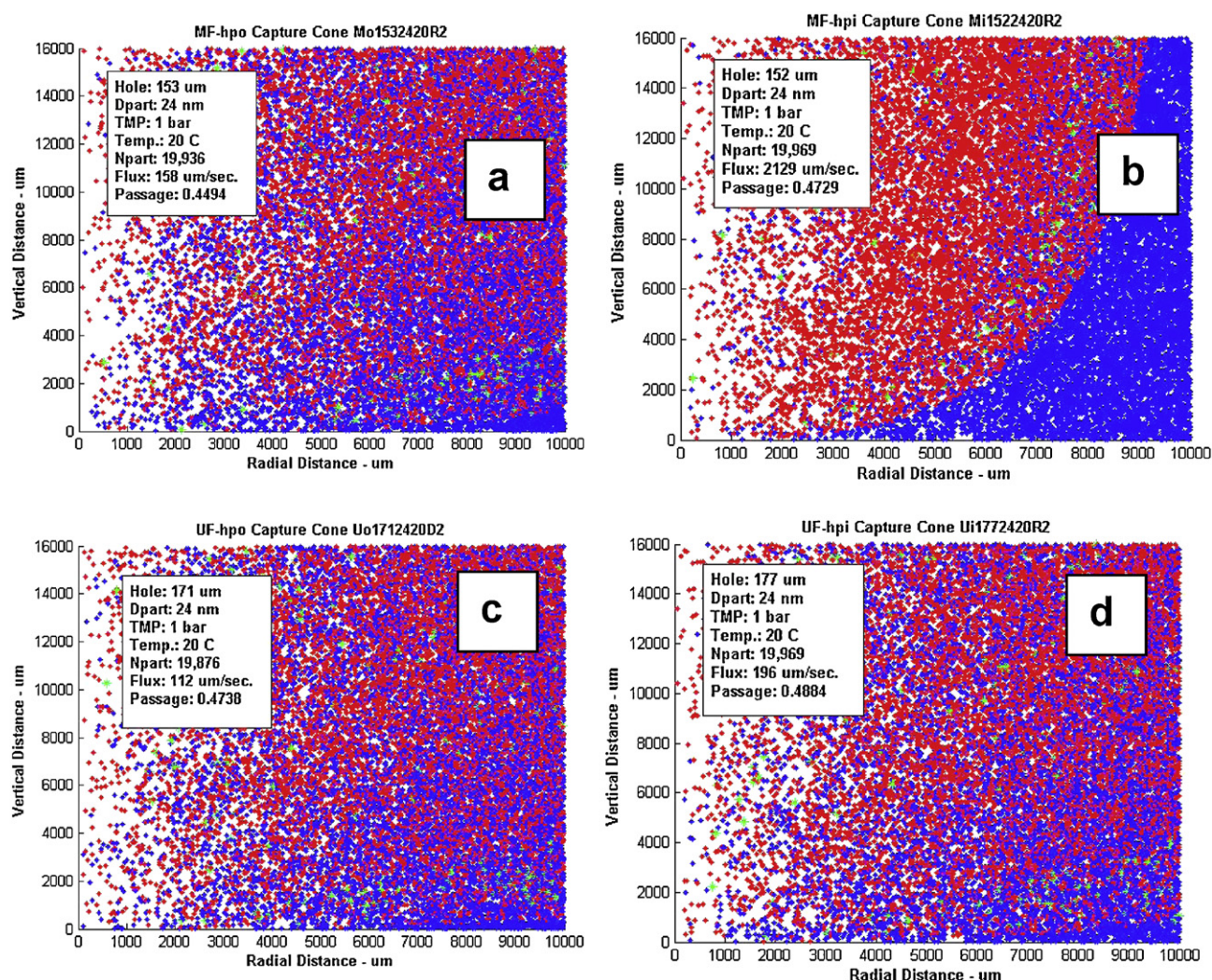


Fig. 8. Large-hole capture cones.

mental protocol and methods used for these challenge studies have been described [15]. A clean membrane specimen was used for each challenge test.

4. Results and discussion

Overall phage rejection results from challenge studies on uncompromised membranes are presented in Fig. 7. These results agree well with phage rejection data presented in the literature [1]. The MF-hpi membrane demonstrated the poorest rejection for both MS2 and PRD1, whereas the UF-hpi membrane demonstrate the highest rejection. As expected, the uncompromised UF membranes were more effective in rejecting viruses than the uncompromised MF membranes.

Simulations were performed using a control volume representing the entire cell volume of phage challenge solution and the experimental conditions used for the phage rejection studies (TMP = 1 bar, $T = 20^\circ\text{C}$). The hole sizes selected correspond to the needle holes created in the corresponding membrane during virus rejection studies. The fractional phage hole passage estimated by the hydrodynamic model represents the fraction of phage that would be expected to pass through the hole in the cell experiments. Examples of fractional hole passage for this control volume is estimated to be 0.4494 (Fig. 8a), 0.4729 (Fig. 8b), 0.4738 (Fig. 8c), and 0.4884 (Fig. 8d) for the MF-hpo, MF-hpi, UF-hpo, and UF-hpi mem-

branes, respectively. These small differences in model estimates result from differences in large hole diameter and membrane thickness. In Fig. 8 each red dot represents a particle that eventually passed through the hole in the membrane, each blue dot represents a particle that eventually passed through the membrane, and each green dot represents a particle that remained in the bulk solution above the membrane surface.

The capture cone shape differs between membranes. The MF-hpi membrane capture cone has the clearest demarcation between the particles passing through the hole and the particles reaching the membrane surface. Recall that this membrane demonstrated the highest flux, more than $10\times$ greater than the other three membranes. A high flux (vertical velocity) relative to the “pull” of the hole and the particle diffusion coefficient yielded a clearly defined capture cone (Fig. 8b). The lower the vertical flux, the more significant the affect of Brownian motion, resulting in a more diffuse capture cone. The MF-hpo membrane had the lowest fractional hole passage, but the UF-hpi capture cone is the most diffuse. Note that in all cases, a few of the particles (green) did not reach either the hole or membrane surface, but remained above both. The calculated diffusion coefficient is $19\ \mu\text{m}^2/\text{s}$ at 20°C for a 24 nm particle.

Model simulations were performed for each membrane using the experimental conditions corresponding to the challenge experiments. Simulation results were used to predict phage rejection for the challenge tests. A comparison of model log rejection predic-

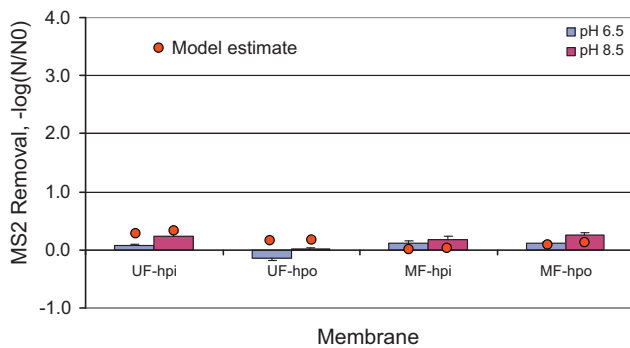


Fig. 9. Comparison of particle tracking model estimates with MS2 rejection experimental results.

tions and phage rejection results for compromised membranes is provided in Figs. 9 and 10. In general, the model overestimated rejection by UF membranes, while estimating reasonably well the rejection by MF membranes. pH was not found to have a significant effect on virus rejection, as shown in Figs. 9 and 10. The lowest pH tested (6.5) is still well-above the isoelectric point of MS2 (3.9) and PRD1 (4.2) and the zeta potential of MS2 and PRD1 are similar at pH 7.5 [15].

Flat sheet and hollow fiber membranes are typically rated based on a nominal pore size, but each membrane exhibits a unique pore size distribution [16]. Urase et al. [17] attributed virus leakage through UF membranes to the presence of abnormally larger pores that are not included in the nominal pore size distribution. Note that the particles shown on the surface of the UF-hpo membrane SEM image (Table 1) are extraneous debris. The likelihood of larger pores in the UF membranes that are not reflected in the nominal pore size rating would allow more passage of phage than the hydrodynamic model would predict.

Simulation results were compared to determine the effect of virus size on fractional hole passage. Virus size had a small effect, and in general, the larger the particle the lower the fractional hole passage. Note that larger viruses (64 nm or greater) have a lower calculated diffusion coefficient (discussed below), and the stochastic component of the hydrodynamic model is less of a factor than for the small virus (24 nm).

An important consideration in conducting virus challenge studies is dispersion of the virions. For purposes of this analysis, the linear distribution of virus particle suspensions simulated in the hydrodynamic model was assumed to be monodispersed (no clumping). A Matlab script was written and applied on selected hydrodynamic model suspensions to calculate the distance between virus particles. In every case, distances between

virus particles were much greater than would be required for significant particle–particle interaction.

The virus challenge solutions used for the bench cell experiments were monodispersed. Virus particles in water are negatively charged and will be held apart by repulsive forces [18]. A 1:1 electrolyte solution was used with an ionic strength of 0.01, hence, the electrical double layer would extend only about 30 Å out into the bulk solution. Attractive van der Waals forces extend only about 10 Å out into the bulk solution. A phosphate buffer was used to maintain the challenge solution pH at 7.5, which is at least 2 pH units greater than the isoelectric point of MS2 and PRD1 phage. Under these conditions, the phage will remain monodispersed even at high concentrations [19]. At a concentration of 10^{10} per mL, virus spacing is still very large, greater than 4000 nm apart for MS2 and PRD1. The phage challenge studies were conducted at phage concentrations of 10^6 to 10^8 . In addition, no organic matter was added nor any coagulant.

The ultimate fate of the virus (hole versus membrane) is affected by the stochastic component of virion movement (Brownian motion). For MF membranes, the vertical water velocity will increase at the membrane surface because of the constricted flow area through the pores. The viruses are smaller than the nominal MF pore size and thus are expected to enter the membrane pore structure, unless the viruses are passively transported through the hole. Because the membrane surface is negatively charged, virus particles will be repulsed as they approach the membrane [20]. Bowen and Sharif [20,21] define the critical velocity as that where the repulsive forces between virions above the membrane are balanced by the hydrodynamic drag forces of the water flowing around the virion. Experimental flux rates used here far exceeded this critical velocity, thus virions would be carried into the MF membrane, where removal would occur due to entrapment and to some degree adsorption [22].

For UF membranes, the nominal pore size is typically smaller than the virions being removed and 100 percent retention is expected at the UF membrane surface. Although it appears smooth under SEM, the UF membrane has surface roughness caused by the ridges around the pore openings. A virus particle reaching the surface of a UF membrane will be “held” in place by the drag force created by the vertical flux velocity as water must pass around the virion, and must flow faster to enter the membrane pores. Hence, membrane roughness causes frictional drag forces as water flow from above pushes downward that will hold the virus in place, while near the hole a cross-flow resulting from the hole will tend to pull the virion sideways.

Hydrodynamic model simulations were performed to determine the radial distance at which $u/v = 1$. Because the y-direction velocity (v) decreases the greater the vertical distance a virion is above the hole, the radial distance at which $u/v = 1$ will also decrease as y increases. Hence, above the hole a lens-shaped area exists within which $u/v > 1$, where virions will be pulled more toward the hole than to the membrane. The size of this lens increases with membrane resistance (R_m). Fig. 11 compares the radial and vertical distance to the lens boundary (or transition boundary) for the membranes examined. The radial distance to the transition zone boundary is the radial distance (x) to the point at which $u/v = 1$, whereas the vertical distance is the distance (y) above the membrane. Note again that even though $u/v > 1$, a virion may still pass through the membrane because of the stochastic component of virion movement. Nevertheless, the smaller the lens the smaller affect of diffusion on the size of the capture cone. Based on this figure, the more hydrophobic membranes (UF-hpo and MF-hpo) as well as the smaller pore UF membrane (UF-hpi) would be expected to have the more diffuse capture cones (i.e., diffusion has a greater effect), which is consistent with model simulations.

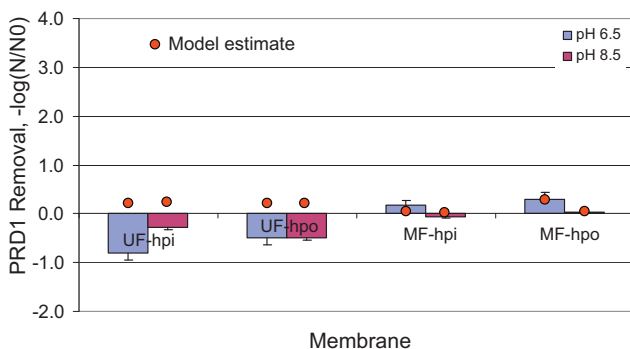


Fig. 10. Comparison of particle tracking model estimates with PRD1 rejection experimental results.

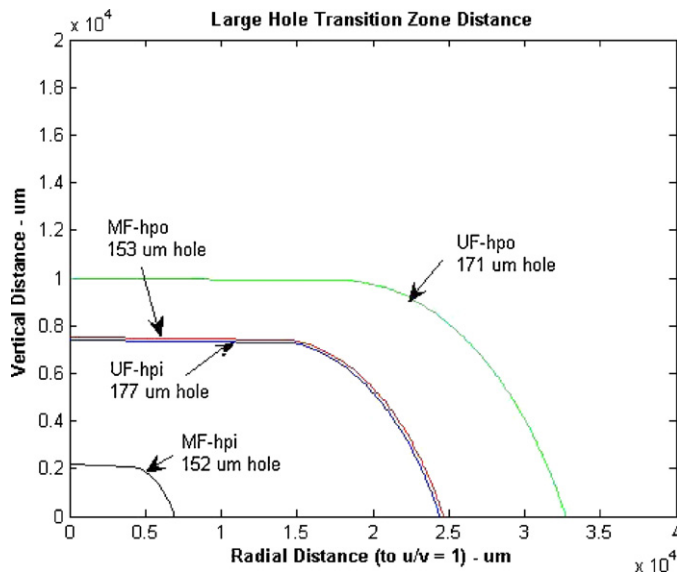


Fig. 11. Radial distance to the transition boundary ($u/v = 1$) as a function of vertical distance for a large hole.

The relative effect of Brownian motion may be generally considered by comparing the relative travel time for advective transport of a virion to the membrane surface, to the relative travel time for diffusion to the hole. The characteristic time of travel (T_{advec}) downward across the control volume to the membrane surface may be calculated as

$$T_{advec} = \frac{h}{Q/A} \quad (29)$$

where h is the height of the control volume (μm), Q is the flow ($\mu\text{m}^3/\text{s}$), and A is the membrane area (μm^2).

The characteristic time of travel (T_{diff}) across the control volume by diffusion to the hole may be calculated as

$$T_{diff} = \frac{\bar{x}^2}{D} \quad (30)$$

where \bar{x}^2 is the mean squared distance traveled (μm^2) and D is the diffusion coefficient ($\mu\text{m}^2/\text{s}$).

The characteristic length traveled for T_{diff} calculation is the radius of the control volume.

As particle size increases, the diffusion coefficient decreases, as indicated in Table 2.

A dimensionless ratio (Φ) provides an indication of the relative significance of the characteristic time for advective transport to diffusive transport

$$\Phi = \frac{T_{advec}}{T_{diff}}$$

As D decreases or the flux (Q/A) increases, Φ increases, and diffusive transport becomes less important. This is illustrated by comparing Φ values summarized in Table 3. The value of Φ for

Table 2
Calculated diffusion coefficients.

Temperature ($^{\circ}\text{C}$)	Calculated diffusion coefficient	
	MS2 phage (24 nm diameter) ($\mu\text{m}^2/\text{s}$)	PRD1 phage (64 nm diameter) ($\mu\text{m}^2/\text{s}$)
4	11	4
10	13	5
15	16	6
20	19	7
25	23	9

Table 3
Values of Φ for large hole simulations.

Membrane	Φ	
	MS2 phage (24 nm diameter)	PRD1 phage (64 nm diameter)
UF-hpi	1.55×10^{-5}	5.71×10^{-6}
UF-hpo	2.71×10^{-5}	1×10^{-5}
MF-hpi	1.43×10^{-6}	5.26×10^{-7}
MF-hpo	1.2×10^{-5}	4.43×10^{-6}

the MF-hpi membrane is approximately an order of magnitude smaller than the other membranes. The MF-hpi membrane consistently demonstrated the highest flux and clearest capture cone. For any particular membrane, Φ will decrease as the virus diameter is increased.

Virus size was found to have a very small effect on hole passage. In general, an increase in virus size slightly lowers passage. Addition of a coagulant is expected to increase virus rejection of the uncompromised membrane by virtue of floc formation and rejection, decreasing virus hole passage. Addition of organic matter is expected to increase virus rejection of the uncompromised membrane by virtue of greater membrane fouling, which would increase membrane resistance and may increase hole passage. An organically fouled membrane will have a higher resistance, but the TMP must be increased if flux is to be maintained, increasing fluid flow through the hole.

5. Conclusions

A hydrodynamic model using a numerical particle-tracking method was developed and applied to describe virus passage through compromised membranes. Large numbers of viruses may potentially pass through compromised membrane surfaces. Low pressure membranes are rated according to nominal pore size, but larger pore openings and imperfections are also present. The hydrodynamic model reasonably predicted the results of large hole stirred cell (deadend) filtration experimental results. Catastrophic failure of compromised membrane was observed in laboratory experiments and predicted by the hydrodynamic model.

For any given set of operating conditions, a “capture cone” defines the extent of hole influence. A proportion of viruses within the cone will pass through the hole. Membrane resistance has the largest effect on the size and extent of influenced of this capture cone.

For a given membrane (R_m), hydrodynamics as determined by flux and hole flow has the largest effect on capture cone size. Flux and hole flow are principally functions of TMP, water temperature, and membrane resistance. Increasing TMP (and flux) generally decreases the size of the capture cone and lowers the fraction of particle hole passage, but only by a small amount. Decreasing water temperature (and flux) generally increases the size of the capture cone.

Viruses of interest in drinking water are small enough such that Brownian motion is a factor in hole passage as a result of diffusive transport. High resistance, low flux conditions generally increase virus passage and the spread of the capture cone.

Acknowledgements

The research reported here was performed while Fred Pontius was a doctoral candidate at the University of Colorado, Boulder. The author thanks the anonymous peer-reviewers of the draft manuscript for their comments which helped to improve the final paper.

Nomenclature

A	surface area of the membrane, cm^2
C	constant of integration
D	diffusion coefficient, cm^2/s
D_{part}	particle diameter, nm
∇	gradient operator
h	height of the control volume, μm
J_{tm}	permeate membrane flux, $\text{L}/\text{m}^2/\text{h}$
k	Boltzmann's constant, J/K
l	tube length, μm
m	strength of ideal point sink
MF-hpi	hydrophilic microfiltration membrane
MF-hpo	hydrophobic microfiltration membrane
Δp	pressure drop, Pa or bar
ϕ	velocity potential
Φ	dimensionless number, $T_{\text{advec}}/T_{\text{diff}}$
Q	flow, L/s or $\mu\text{m}^3/\text{s}$
Q_y	flow in y -direction, L/s
r	radius, μm
r_s	solute radius, nm
R	tube radius, μm
R_m	membrane resistance, $(\text{bar h m}^2)/(\text{L cp})$
R_t	total resistance of the membrane, $(\text{bar h m}^2)/(\text{L cp})$
S	sphere surface
θ	angular displacement
t	time, s
Δt	time step, s
T	temperature, $^\circ\text{C}$
T_{advec}	characteristic time of particle travel due to advection, s
T_{diff}	characteristic time of particle travel due to diffusion, s
TMP	transmembrane pressure, bar
T_{step}	time step used for simulations, s
μ	absolute viscosity, cp
u	x -direction velocity, $\mu\text{m}/\text{s}$
\vec{u}	velocity vector at position x_{n-1}
UF-hpi	hydrophilic ultrafiltration membrane
UF-hpo	hydrophobic ultrafiltration membrane
v	y -direction velocity, $\mu\text{m}/\text{s}$
v_r	radial velocity, $\mu\text{m}/\text{s}$
v_θ	angular velocity, rad/s
v_z	z -direction velocity, $\mu\text{m}/\text{s}$
\mathbf{V}	velocity vector
w	z -direction velocity, $\mu\text{m}/\text{s}$
x	radial distance, μm
x_{Max}	maximum x distance for the control volume
x_{Min}	minimum x distance for the control volume
\vec{x}_n	particle position vector
y	vertical distance, μm

y_{Max}	maximum y distance for the control volume
y_{Min}	minimum y distance for the control volume
ζ	vorticity
z	z -direction distance
Z	a two-dimensional vector of random numbers with mean magnitude zero and variance one

References

- [1] USEPA, Membrane Filtration Guidance Manual, EPA 815-R-06-009, Office of Water, Washington, DC, 2005.
- [2] H. Guo, Y. Wyart, J. Perot, F. Nauleau, P. Moulin, Low-pressure membrane integrity tests for drinking water treatment: a review, *Water Res.* 44 (2010) 41–57.
- [3] B. Mi, B.J. Marinas, J. Curl, S. Sethi, G. Crozes, D. Hugaboom, Microbial passage in low pressure elements with compromised integrity, *Environ. Sci. Technol.* 39 (2009) 4270–4279.
- [4] W. Kinzelbach, The random walk method in pollutant transport simulation, in: E. Custodio, et al. (Eds.), *Groundwater Flow and Quality Modelling*, D. Reidel Publishing Company, Dordrecht, 1988.
- [5] C.F. Scott, Particle tracking simulation of pollutant discharges, *J. Environ. Eng.* 123 (1997) 919.
- [6] W.E. Hathhorn, Simplified approach to particle tracking methods for contaminant transport, *J. Hydr. Eng.* 123 (1997) 1157.
- [7] A. Tompson, L. Gelhar, Numerical simulation of solute transport in three-dimensional, randomly heterogeneous porous media, *Water Resour. Res.* 26 (1990) 2541.
- [8] J.P. Crimaldi, J.R. Hartford, J.B. Weiss, Reaction enhancement of point sources due to vortex stirring, *Phys. Rev. E* 74 (2006), Art. No. 016307 Part 2.
- [9] K. Dimou, E. Adams, A random-walk, particle tracking model for well mixed estuaries and coastal waters, *Estuar. Coast. Shelf Sci.* 37 (1993) 99.
- [10] J.P. Crimaldi, H.S. Browning, A proposed mechanism for turbulent enhancement of broadcast spawning efficiency, *J. Marine Syst.* 49 (2004) 3.
- [11] A. Einstein, *Investigations in the Theory of the Brownian Movement*, Dover, New York, 1956.
- [12] P. Hiemenz, R. Rajagopalan, *Principles of Colloid and Surface Chemistry*, Marcel Dekker, Inc., New York, 1997.
- [13] J.W. Möller, Determination of diffusion coefficients and molecular weights of ribonucleic acids and viruses, *Biochemistry* 51 (1964) 501.
- [14] A.R. Badireddy, S. Chellam, Diffusivity measurements of bacteriophages by gradient diffusion and dynamic light scattering, in: *Proceedings of the 2006 Annual Conference of the American Institute of Chemical Engineers*, San Francisco, CA, 2006.
- [15] F. Pontius, G. Amy, M. Hernandez, Fluorescent microspheres as virion surrogates in low-pressure membrane studies, *J. Membrane Sci.* 335 (2009) 43–50.
- [16] C. Zhao, X. Zhou, Y. Yue, Determination of pore size and pore distribution on the surface of hollow-fiber filtration membranes: a review of methods, *Desalination* 129 (2000) 107.
- [17] T. Urase, K. Yamamoto, S. Ohgaki, Effect of pore structure of membranes and module configuration on virus rejection, *J. Membrane Sci.* 115 (1996) 21.
- [18] C. Gerba, Applied and Theoretical Aspects of Virus Adsorption to Surfaces, *Adv. Appl. Microbiol.* 30 (1984) 133.
- [19] R. Floyd, D.G. Sharp, Aggregation of poliovirus and reovirus by dilution in water, *Appl. Environ. Microbiol.* 33 (1977) 159.
- [20] W. Bowen, A. Sharif, The hydrodynamic and electrostatic interactions on the approach and entry of a charged spherical particle to a charged cylindrical pore in a charged planar surface with implications for membrane separation processes, *Proc. R. Soc. (Lond.) A* 452 (1996) 2121.
- [21] W. Bowen, A. Sharif, Hydrodynamic and electrostatic interactions effects on the rejection of a particle larger than a pore in microfiltration and ultrafiltration membranes, *Chem. Eng. Sci.* 53 (1998) 879.
- [22] J. Jacangelo, S. Adham, J.-M. Laine, Mechanism of cryptosporidium, giardia, and MS2 virus removal by MF and UF, *J. AWWA* 81 (1995) 107.